PROCEEDINGS B

rspb.royalsocietypublishing.org

Research

Cite this article: Ronellenfitsch H, Liesche J, Jensen KH, Holbrook NM, Schulz A, Katifori E. 2015 Scaling of phloem structure and optimality of photoassimilate transport in conifer needles. *Proc. R. Soc. B* **282**: 20141863.
http://dx.doi.org/10.1098/rspb.2014.1863

Received: 28 July 2014
Accepted: 4 December 2014

Subject Areas:
plant science, theoretical biology

Keywords:
phloem structure, photoassimilate transport, optimization, mathematical modelling

Author for correspondence:
Henrik Ronellenfitsch
e-mail: henrik.ronellenfitsch@ds.mpg.de

Electronic supplementary material is available at http://dx.doi.org/10.1098/rspb.2014.1863 or via http://rspb.royalsocietypublishing.org.

THE ROYAL SOCIETY PUBLISHING

Scaling of phloem structure and optimality of photoassimilate transport in conifer needles

Henrik Ronellenfitsch[1], Johannes Liesche[2], Kaare H. Jensen[3,4], N. Michele Holbrook[3], Alexander Schulz[2] and Eleni Katifori[1]

[1]Max Planck Institute for Dynamics and Self-Organization, Am Faßberg 17, 37077 Göttingen, Germany
[2]Department of Plant and Environmental Sciences, University of Copenhagen, 1871 Frederiksberg C, Denmark
[3]Department of Organismic and Evolutionary Biology, Harvard University, Cambridge, MA 02138, USA
[4]Department of Physics, Technical University of Denmark, 2800 Kgs. Lyngby, Denmark

The phloem vascular system facilitates transport of energy-rich sugar and signalling molecules in plants, thus permitting long-range communication within the organism and growth of non-photosynthesizing organs such as roots and fruits. The flow is driven by osmotic pressure, generated by differences in sugar concentration between distal parts of the plant. The phloem is an intricate distribution system, and many questions about its regulation and structural diversity remain unanswered. Here, we investigate the phloem structure in the simplest possible geometry: a linear leaf, found, for example, in the needles of conifer trees. We measure the phloem structure in four tree species representing a diverse set of habitats and needle sizes, from 1 (*Picea omorika*) to 35 cm (*Pinus palustris*). We show that the phloem shares common traits across these four species and find that the size of its conductive elements obeys a power law. We present a minimal model that accounts for these common traits and takes into account the transport strategy and natural constraints. This minimal model predicts a power law phloem distribution consistent with transport energy minimization, suggesting that energetics are more important than translocation speed at the leaf level.

1. Introduction

Plants, diverse species of algae and other organisms acquire chemical energy in the form of carbohydrates (sugars) from the sun through photosynthesis. These photoassimilates are exported from plant leaves via the phloem vascular system to support life in distal parts of the organism. The flow is driven by a build-up of osmotic pressure in the veins, where high concentrations of sugar direct a bulk flow of sweet sap out of the leaf. The vascular network is critical to sustenance and growth; more subtly, it is also of importance as a carrier of signalling molecules that integrate disparate sources of information across the organism. The mechanisms that influence phloem structure to fulfil these multiple objectives, however, remain poorly understood.

The phloem is a complex distribution system responsible for transporting a large number of organic molecules, defensive compounds and developmental signals by bulk fluid flow through a network of elongated sieve element cells which are connected to each other by porous sieve plates, effectively forming long tubes [1]. The phloem thus serves functions analogous to a combination of the nervous and circulatory systems of animals. The role of the phloem in the transport of photoassimlates has been known since the seventeenth century [2], but it was not until 1930 that the role of the phloem sieve element as the channel of carbohydrate transport in plants was experimentally demonstrated [3–5]. Although the primary role of phloem transport is to distribute the products of photosynthesis, it also plays a role in long-distance transmission of signals for some developmental and environmental responses. For instance, flowering is induced by transmission of a phloem-mobile hormone from the leaves to the meristem [6]. In addition,

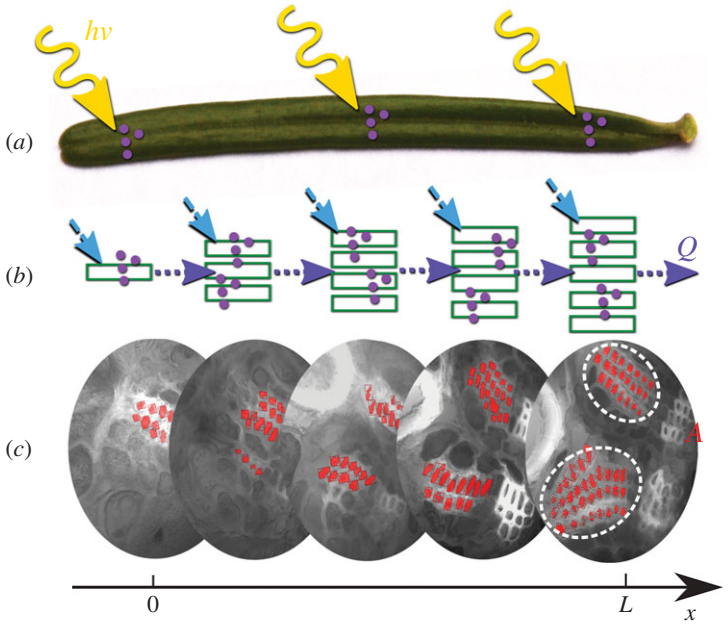

Figure 1. Phloem geometry in a conifer needle. (*a*) Schematic of a photosynthesizing *A. nordmanniana* needle. (*b*) The mechanism driving sugar export in plant leaves. Sugar molecules (purple dots) are produced via photosynthesis and diffuse into the phloem cells. The osmotic sugar solution attracts water from the surrounding tissue (blue dashed arrows) which generates a bulk flow $Q(x)$ along the needle (purple dotted arrows). (*c*) Micrograph cross sections of the phloem of an *A. nordmanniana* needle taken at distances $x = 0.4, 0.8, 1.6, 2.9, 4.9$ mm from the tip. The diameter of the circular cross sections is 100 μm. The conductive phloem area $A(x)$ (red cells) increases with distance x from the needle tip, whereas the size of individual cells is roughly constant. (Online version in colour.)

pathogen protection and related gene expression signals have been shown to occur through the phloem [6].

Phloem flow occurs in an interconnected network of long, narrow cylindrical cells. In these cells, an energy-rich solution of sap containing 10–30% wt sugars flows towards distal regions of the plant [7]. Transport is driven by the osmotic Münch pump [7–12]. The flow is initiated in the leaf, where sugars produced by photosynthesis accumulate in phloem cells. This induces an osmotic gradient with respect to the surrounding tissue, drawing in water into the phloem cells. On the scale of the phloem tissue, this process results in a bulk flow of sap along the major veins out of the leaf, towards regions of low osmotic potential in the plant, such as roots or fruits. Münch flow in a conifer needle is sketched in figure 1, where the phloem tissue is located within a single large vein near the centre of the leaf cross-section plane. Close to the tip of the needle, only few sieve tubes exist to support the flow of sap, more continually being added to the bundle as one moves closer to the petiole. Neighbouring sieve tubes maintain hydraulic connections through plasmodesmata.

The driving force responsible for carbon export is the steady production of photosynthate in the leaf mesophyll located close to the leaf surface. The mechanism by which sugars accumulate in the phloem varies between species. Most plants, however, can be roughly divided into two groups: active and passive phloem loaders [13]. Active loaders use membrane transporters or sugar polymerization to accrue carbon in the phloem, whereas passive loaders rely on cell-to-cell diffusion aided by bulk flow through plasmodesmata pores [13–15]. Trees are predominantly passive loaders, whereas many herbaceous plants use active phloem loading [13–16].

The quantity of material exported through the phloem is generally assumed to be strongly dependent not only on physiological factors such as solar radiation intensity and water availability [17,18], but it also likely to depend on details of the leaf vascular architecture. For instance, the positioning and network structure of water-transporting xylem conduits in plant stems and leaves has been shown to play an important role in determining the efficiency of CO_2 uptake [19–24]. While the branched vein network architecture in plant leaves has been studied extensively, less is known about the functional elements. Except for a few species of grasses, which have a parallel vein geometry similar to needles [25–27], the detailed functional architecture of the phloem (i.e. the location, number and size of conducting elements) in plant leaves remains unknown, in part, owing to the high sensitivity of phloem tissue to disturbances [28].

In this work, we aim to answer two basic questions. First, we ask what is the design of the phloem vascular system in conifer needles, i.e. what are its geometric and hydrodynamic properties. Second, we aim to determine whether the observed structure is consistent with energy minimization or maximizing flow rate to elucidate the selective force that influences phloem structure. We chose conifer needles for this study, in part, owing to their linear structure without branching veins, a geometrical feature which greatly simplifies the analysis of the transport process. Moreover, conifer trees inhabit diverse environments, and the vascular network has thus been subjected to a broad selective pressure. Accordingly, we present the experimental results of phloem geometry in needles of four conifer species from a diverse set of habitats and needle sizes. Based on these, we develop a minimal mathematical model of sugar transport in leaves, and use a constrained optimization to derive the optimal phloem geometry in a one-dimensional leaf. Finally, we compare modelling with experimental results, and conclude by discussing the implications of our results for the study of conifers and plants in general.

2. Results

(a) Phloem structure

We measured the phloem geometry in needles of four conifer species shown in figure 2: *Abies nordmanniana*, *Pinus palustris*,

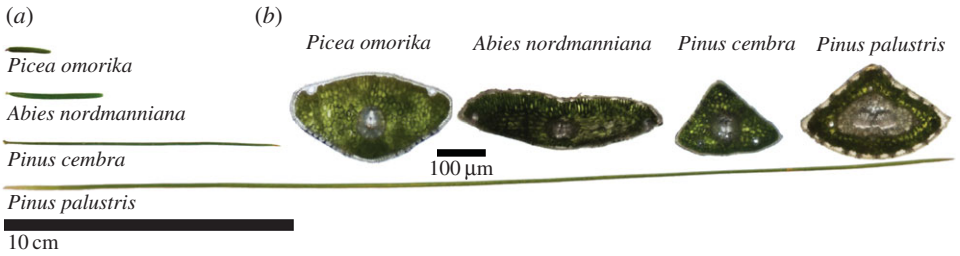

Figure 2. Conifer needle characteristics. (*a*) Photographs of representative needle specimens of the species studied in this work. Typical lengths range between 1 and 30 cm. From top to bottom, *Picea omorika*, *Abies nordmanniana*, *Pinus cembra*, *Pinus palustris*. (*b*) Micrographs showing cross sections of a typical needle specimen. The vascular tissue in the centre of each specimen (light colour) is clearly discernible. (Online version in colour.)

Pinus cembra and *Picea omorika*. Three to six needles were sampled from each species. The species encompass the range of typical needle sizes of conifer species, from *P. omorika* (needle length $L \sim 1$ cm) to *P. palustris* ($L \sim 35$ cm). Additionally, they incorporated plants from diverse habitats and climates ranging from *P. palustris*, whose habitats are the Gulf and Atlantic coastal plains of the USA, to the European alpine *P. cembra*. The measurements were conducted by performing transverse sections at 10–20 positions along the length of the needle. Phloem cells were identified by the presence of a stain as described in the Materials and methods section. A typical stack of images obtained this way is shown in figure 1*c*.

To quantify the phloem structure, we measured the size of all sieve elements in each cross section. Starting from the tip of the needle, we typically observed an increase in the total conductive area A towards the base of the leaf (figure 3*a*). The cross-sectional area of individual sieve elements a (figure 3*b*), however, shows only minimal variation as a function of length (correlation to position using Pearson's $|r| < 0.23$ for all needles in figure 3*b*), implying that the main variation in transport area is driven by changes in the number of conduits N. When the total phloem transport area is normalized and plotted relative to the needle length L on logarithmic axes (figure 4), it is seen to behave roughly as a power law $A/A(L) \sim (x/L)^{\alpha}$ with average exponents per species between $\alpha = 0.45$ (*P. omorika*) and $\alpha = 0.56$ (*A. nordmanniana*; table 1). The number of sieve elements $N(x) \sim x^{\alpha}$ follows a similar scaling with $\alpha \approx 1/2$. Because the cross-sectional area of individual sieve elements is nearly constant, this result is to be expected.

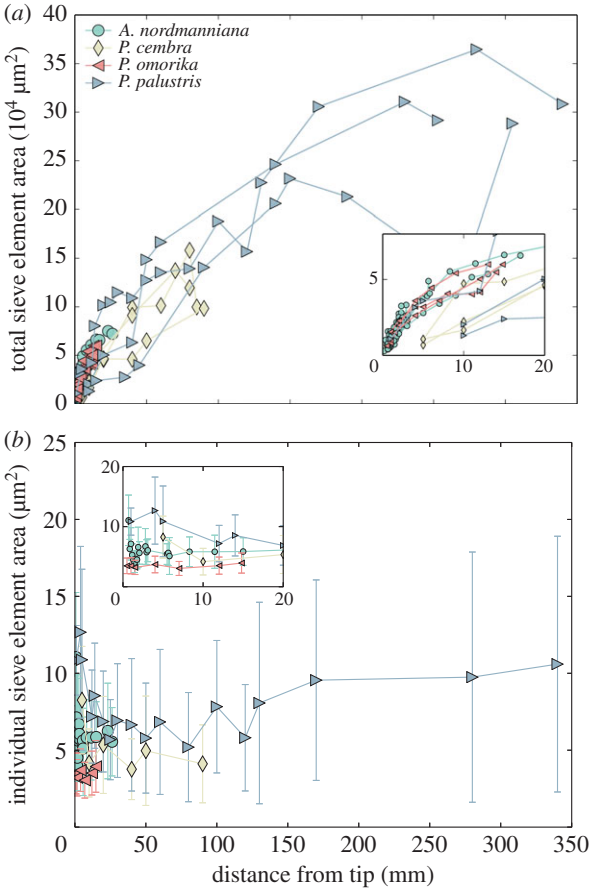

Figure 3. Phloem area increases with distance from the needle tip. Total conductive phloem area A, shown in (*a*) for all analysed needles, and cross-sectional area of individual sieve elements a, shown in (*b*) for one needle of each species, as a function of distance x from the needle tip for the conifer species indicated in the legend (see also figure 2). Error bars in (*b*) correspond to one standard deviation. The individual sieve element areas show only little variation as a function of position, as evidenced from Pearson's $|r| < 0.23$ for all needles shown, implying that it is mainly the number of sieve elements which contributes to hydraulic efficiency. Data from individual needles are connected by solid lines. Insets show details near $x = 0$ for the shorter species. (Online version in colour.)

(b) Mathematical model for sugar transport in plants

To rationalize the observed vein structure, we develop a simple model of one-dimensional sugar transport in a bundle of parallel phloem tubes based on the work of Horwitz [8] and Thompson & Holbrook [9]. Sugar flow commences near the needle tip $x = 0$, where a few phloem conduits initiate the export of photoassimilates. Approaching the needle base ($x = L$), the number of conducting channels N increases, whereas the size of individual phloem tubes remains constant. Because the length scale at which N varies is small compared with the total length L of the needle, we can approximate N well by a smooth function. We note that the precise way in which the number of sieve tubes changes (be it by simple addition of new tubes or branching of existing ones) has no impact on the continuum description. Phloem loading in conifers is thought to be passive, driven by cell-to-cell diffusion across microscopic (plasmodesmata) channels [16]. The sugar loading rate per unit length of needle Γ is proportional to the rate of photosynthesis and to the circumference of the needle, both of which are approximately constant along the needle (figure 2). For a collection of parallel phloem tubes, conservation of sugar mass can be expressed as

$$\frac{\mathrm{d}J}{\mathrm{d}x} = \Gamma, \tag{2.1}$$

where $J(x) = Q(x)c(x)$ is sugar current with $Q(x)$ the total volume flow rate, and $c(x)$ is the sap sugar concentration.

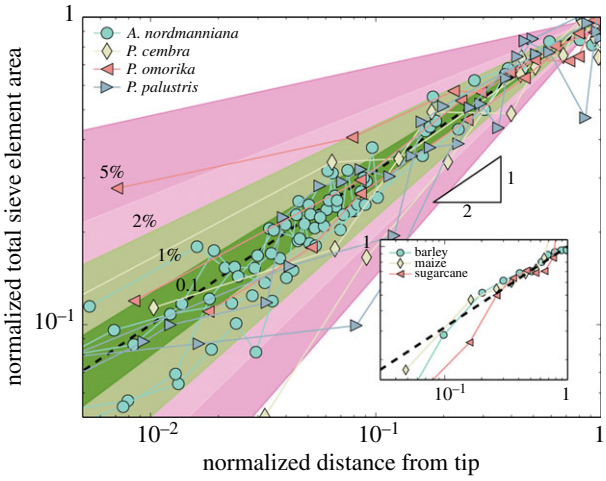

Figure 4. Conifer needle phloem follows the $\alpha = 1/2$ law. Phloem area $A/A(L)$ plotted as a function of distance from the needle tip x/L on double-logarithmic axes. The dashed line has slope 1/2. The coloured regions correspond to all power laws $A_\alpha(x) \sim (x/L)^\alpha$ whose power dissipation exceeds that of the optimal solution $A_{1/2}$ by the given percentages. Most of the needles analysed fall within the 1% range $\alpha \in [0.35, 0.65]$ (table 1). The inset shows phloem area data from the monocots barley, maize and sugarcane obtained from [25–27]. Barley is in good accord with the $\alpha = 1/2$ scaling, whereas maize and sugarcane also only show approximate sublinear dependences on distance from leaf tip. (Online version in colour.)

We further assume that at each point water enters the sieve elements by osmosis

$$\frac{dQ}{dx} = 2\frac{L_p A}{r_0}(RT\Delta c - \Delta p), \tag{2.2}$$

where $A(x)$ is the total conductive phloem area at the position x (see figure 1 for visualization). Note that $A(x) = N(x)A_0$, where $N(x)$ is the number of sieve tubes at position x and A_0 is the cross-sectional area of a single sieve tube. In equation (2.2), L_p denotes the permeability of the sieve element membrane, R is the universal gas constant, T is the absolute temperature and r_0 is the radius of one single sieve element. The sugar concentration $\Delta c = c(x) - c_1$ available for driving an osmotic flow is the difference between the concentration in the sieve element c and the constant osmotic concentration c_1 of the surrounding cells. Likewise, the pressure $\Delta p = p(x) - p_1$ is the difference between the cytoplasmic pressure p and the constant pressure in neighbouring cells p_1. For clarity, we use the van't Hoff value $RT\Delta c$ for the osmotic pressure in equation (2.2), which is valid only for dilute (ideal) solutions. At the concentrations relevant to phloem sap ($c \leq 1$ M), the error in the osmotic pressure introduced by using the van't Hoff value is ≈10% [29]. Equation (2.1) may be integrated to yield $J(x) = \Gamma x$, having imposed a vanishing current at the tip. The total export of sugar from the needle is therefore $J(L) = \Gamma L$, proportional to the loading rate Γ and needle length L. The factors contributing to the energetic cost of transport include the metabolic energy required to maintain the vasculature and the power dissipated by the flow owing to viscous friction. We proceed to consider how the phloem structure influences the magnitude of these contributions, and note that similar energy considerations have been used in the study of other biological transport systems [23,30–32]. For instance, Zwieniecki *et al.* [23] derived the optimal distribution of tracheids in a pine needle that minimizes the pressure drop required to drive transpiration for a given

Table 1. Results of least-squares fitting total sieve tube area $\log A(x) = c + \alpha \log x$ for individual needles. Asterisks highlight significance levels (***$p < 0.001$, **$p < 0.01$, *$p < 0.05$), error estimates given correspond to one standard deviation.

species	scaling exponent α	R^2	p value
Pinus palustris			
	0.51	0.94	<0.001***
	0.60	0.90	<0.01**
	0.67	0.82	<0.001***
average	0.59 ± 0.06		
Abies nordmanniana			
	0.38	0.71	<0.001***
	0.65	0.95	<0.001***
	0.72	0.92	<0.001***
	0.48	0.84	<0.01**
	0.48	0.92	<0.001***
	0.65	0.99	<0.001***
average	0.56 ± 0.12		
Pinus cembra			
	0.73	0.92	<0.001**
	0.41	0.95	<0.01**
	0.61	0.91	<0.05*
average	0.58 ± 0.13		
Picea omorika			
	0.30	0.92	<0.001***
	0.47	0.98	<0.001***
	0.58	0.99	<0.001***
average	0.45 ± 0.11		

investment in xylem conduit volume. The phloem consists of severely reduced cells which shed most of their organelles during maturation. It is, however, alive and relies on an external supply of metabolic energy. The rate of energy consumption by the phloem tissue itself may be seen as an energetic maintenance cost of the transport conduit. Here, we assume that this energetic cost of maintaining the phloem vasculature is proportional to the conductive volume $V_0 = \int_0^L A(x)\,dx$, or equivalently the number of phloem cells (assuming cells of roughly equal size). The viscous power dissipation per unit length is $dW = -(Q\,dp + p\,dQ)$. To determine W, we note that the local pressure gradient is related to the flow speed $u = Q/A$ by Darcy's law

$$u(x) = -\frac{k}{\mu}\frac{dp}{dx}, \tag{2.3}$$

where $p(x)$ is the pressure, μ is the viscosity of phloem sap (typically around five times that of water [33]) and $k = A_0/8\pi$ is a geometrical constant which solely depends on the cross-sectional area A_0 of single sieve elements. Integrating equation (2.1) leads to $J = uAc = \Gamma x$, and thus the local pressure gradient is given by

$$\frac{dp}{dx} = -\frac{\mu}{k}\frac{\Gamma}{c(x)}\frac{x}{A(x)}. \tag{2.4}$$

Analysis of the coupled system in equations (2.1) and (2.2) have shown that the concentration $c(x)$ is approximately constant along the needle $c(x) \approx c_0$ [9,12] (see also the electronic supplementary material). Integrating the differential relation for W using the above set of approximations, the total power dissipation is

$$W = Q(L)\Delta p = \frac{\mu}{k}\frac{\Gamma^2}{c_0^2}\int_0^L \mathrm{d}x\,\frac{x}{A(x)}. \tag{2.5}$$

For a given conductive phloem volume V_0, we can now determine the area distribution $A(x)$ which minimizes the viscous power dissipation. Using the method of Lagrange multipliers and the calculus of variations, one finds that the distribution which minimizes (2.5) under the constraint $\int_0^L A(x)\,\mathrm{d}x = V_0$ is

$$A(x) = \frac{3}{2}\frac{V_0}{L}\left(\frac{x}{L}\right)^{1/2} = \frac{3}{2}\langle A\rangle\left(\frac{x}{L}\right)^{1/2}, \tag{2.6}$$

where $\langle A\rangle$ is the average total area of sieve elements. Assuming a bundle of sieve elements with constant cross-sectional area, this result may be translated immediately to total number of sieve elements by

$$N(x) = \frac{A(x)}{A_0} = \frac{3}{2}\langle N\rangle\left(\frac{x}{L}\right)^{1/2}, \tag{2.7}$$

where A_0 is the cross-sectional area of a single sieve element. From equations (2.6) and (2.7), we conclude that a scaling of phloem sieve element number or area with the power $\alpha = 1/2$ minimizes the viscous power dissipation. The observed scaling exponents (figure 4 and table 1) are close to these values, suggesting that the sieve element areas roughly follow the theoretical optimum. We note that the square-root scaling in equation (2.7) is identical to that found by Zwieniecki *et al.* [23] for the tapering of pine needle xylem conduits. The coupling between water flow and phloem loading required to maintain a constant photosynthetic rate along the needle is thus responsible for driving this remarkable convergence in vascular architecture. In the context of leaf development, we note that pine needles grow from a meristem located at the base of the needle which gradually propels the tip away from the growth zone. Newly formed tissue at the base of the needle gradually becomes mature and loses its ability to change its structure as the needle extends. The distribution of phloem conduits along the needle length thus appears to be either predetermined or rely on exchange of information between the tip of the needle and the meristem.

While our model is not generally applicable to complex reticulate or anastomosing vein networks, we expect it to be suitable for analysis of leaves with parallel veins, given that the assumption of constant sieve element properties is valid. Evidence to support this hypothesis is found in studies by Evert and co-workers [25–27], who observed similar trends in grasses. For example, phloem area in barley, maize and sugarcane roughly follow the $\alpha = 1/2$ law, (figure 4, inset), suggesting that the energy dissipation criterion leading to the prediction $\alpha = 1/2$ is broadly applicable. We show in the appendix that the constant volume constraint imposed when obtaining $\alpha = 1/2$ can be relaxed, and that sublinear scalings is a general feature of the energy minimization principle.

Previous works [11,12], which focused on one-dimensional models of flow in sieve elements, identified the transport velocity (phloem sap flux density) as an important physiological parameter. In fact, optimizing the sieve element radius (r_0 in equation (2.2)) for maximum flux at the whole plant level results in predictions that are in agreement with experimental observations [11]. Interestingly, we find (see the electronic supplementary material) that while the observed conduit distribution (i.e. $A \propto x^{1/2}$) minimizes the energetic cost of transport for a fixed tube radius r_0, it does not maximize the average flux density. The size of individual phloem cells at the level of the whole tree thus appears to be optimized for flux density, whereas the arrangement of tubes in the needle minimizes the energetic cost of transport, working in concert to produce an efficient system of nutrient translocation.

3. Discussion

In this work, we studied the physical properties of nutrient transport in the phloem of conifer needles. We measured the geometrical properties of needle phloem in several conifer species, varying over one order of magnitude in length, and found that their cross-sectional area distribution roughly follows the law $A(x) \sim x^{1/2}$. We presented a simple mathematical model which is able to rationalize the observed needle tube geometry by means of minimization of the energy dissipated during flow. Expenditure of energy is unavoidable because, although, the transport is entirely passive by virtue of the osmotic flow process, the plant is forced to maintain an osmotic gradient, consuming energy in the process. We found that experimental data from several species of conifers agree well with the theoretically derived law of area distribution.

Simple models such as the ones considered in this work may not only elucidate the properties of structures with modest complexity we see in the living world, but also serve as an important stepping stone to further understanding of more complicated systems. The basic underlying constraints and functional requirements that dictate needle design in conifers are not unique to this group of plants. Data from parallel-veined grasses indicate similar trends, and the design requirements are expected to hold for plants with reticulate venation patterns. The same mathematical model can potentially be extended to predict vascular distribution when the leaf lamina is broad and the single vein is replaced by an extensive reticulate network.

The conifer needle belongs to a general class of network systems that follow a principle of energy dissipation minimization. Other important members of this class which is not constrained to one-dimensional or even planar systems include the networks of blood vessels in animals [31,32], the xylem vascular system in plants [21,34] and even river basin networks in geomorphology [35], thus establishing the importance of optimization considerations.

Finally, we point out that in recent years the constructal law, stipulating that all living organisms are built so as to optimally facilitate flow (of fluids, stresses, energy) has enjoyed some success [36,37] in explaining the structure and apparent design of biological systems. The findings we report in this paper appear to be in accordance with the basic ideas from constructal theory.

4. Material and methods

Needles of mature *A. nordmanniana*, *Pinus palustris*, *Pinus cembra* and *Picea omorika* were collected in May and June of 2013. Samples of *A. nordmanniana*, *P. cembra* and *P. omorika* were

taken in Denmark, whereas *P. palustris* needles were collected in Florida (USA) and shipped to Denmark by courier.

Needles were embedded in low-melting point agarose (Sigma-Aldrich) and sectioned with a vibrating blade microtome (Leica Microsystems) to ensure uniform section thickness of 100 µm. Sections were imaged using a confocal laser scanning microscope (SP5X, Leica Microsystems). In this way, three to six needles of average length (figures 1 and 2) from each species were analysed. The number of sieve elements and their cross-sectional area were quantified using the image analysis software VOLOCITY (v. 5.3, PerkinElmer).

By way of fluorescence staining with the live-cell marker carboxy fluorescein diacetate (Sigma-Aldrich), non-functional sieve elements were excluded. Needle sections of 5 mm length were incubated in carboxy fluorescein for 15 min after which sections were made and analysed under the microscope. For all species, only a few strongly deformed sieve elements at the abaxial side of the phloem bundle in which almost no cytoplasm was visible were found to be dead, i.e. non-functional. These cells were not included in the analysis.

Data accessibility. The phloem geometry data are available digitally at Dryad Digital Repository (doi:10.5061/dryad.024bn).

Funding statement. The work of K.H.J. is supported by the Air Force Office of Scientific Research (award no. FA9550-09-1-0188), the National Science Fundation (grant no. DMR-0820484), the Danish Council for Independent Research | Natural Sciences and the Carlsberg Foundation. The work of H.R. is supported by the IMPRS for Physics of Biological and Complex Systems, Göttingen. E.K. acknowledges the support of the Burroughs Wellcome Fund through the BWF Career Award at the Scientific Interface.

Appendix A

We consider an extension of the constant volume constraint by introducing a more general dependency on some power of the total area

$$\int_0^L \mathrm{d}x\, A(x)^\gamma = K, \tag{A 1}$$

where we now think of K as a general cost of building material and metabolism which scales with cross-sectional area in a nonlinear way. Constraints of this type have been used extensively in the field of complex distribution networks [21,38]. The optimization of equation (2.5) under this generalized constraint predicts a scaling of

$$A(x) \sim x^{1/(\gamma+1)}. \tag{A 2}$$

We note that this result is robust: the optimal area scaling is sublinear, whatever the value of the scaling power γ of the cost function.

References

1. Knoblauch M, Peters WS. 2010 Münch, morphology, microfluidics: our structural problem with the phloem. *Plant, Cell Environ.* **33**, 1439–1452.
2. Taiz L, Zeiger E. 2010 *Plant physiology*. Sunderland, MA: Sinauer Associates.
3. Schumacher W. 1930 Untersuchungen über die Lokalisation der Stoffwanderung in den Leitbündeln höherer Pflanzen. *Jahrb. Wiss. Bot.* **73**, 770–823.
4. Mason TG, Phillis E. 1937 The migration of solutes. *Bot. Rev.* **III**, 47–71. (doi:10.1007/BF02872295)
5. Crafts AS, Crisp CE. 1971 *Phloem transport in plants*. San Francisco, CA: W. H. Freeman & Co Ltd.
6. Lough TJ, Lucas WJ. 2006 Integrative plant biology: role of phloem long-distance macromolecular trafficking. *Annu. Rev. Plant Biol.* **57**, 203–232. (doi:10.1146/annurev.arplant.56.032604.144145)
7. Münch E. 1930 *Die Stoffbewegungen in der Pflanze*. Jena, Germany: Verlag von Gustav Fischer.
8. Horwitz L. 1958 Some simplified mathematical treatments of translocation in plants. *Plant Physiol.* **33**, 81–93. (doi:10.1104/pp.33.2.81)
9. Thompson MV, Holbrook N. 2003 Application of a single-solute non-steady-state phloem model to the study of long-distance assimilate transport. *J. Theor. Biol.* **220**, 419–455. (doi:10.1006/jtbi.2003.3115)
10. Pickard WF, Abraham-Shrauner B. 2009 A simplest steady-state Munch-like model of phloem translocation, with source and pathway and sink. *Funct. Plant Biol.* **36**, 629–644. (doi:10.1071/FP08278)
11. Jensen KH, Lee J, Bohr T, Bruus H, Holbrook NM, Zwieniecki MA. 2011 Optimality of the Münch mechanism for translocation of sugars in plants. *J. R. Soc. Interface* **8**, 1155–1165. (doi:10.1098/rsif.2010.0578)
12. Jensen KH, Liesche J, Bohr T, Schulz A. 2012 Universality of phloem transport in seed plants. *Plant. Cell Environ.* **35**, 1065–1076. (doi:10.1111/j.1365-3040.2011.02472.x)
13. Turgeon R. 2006 Phloem loading: how leaves gain their independence. *Am. Inst. Biol. Sci.* **56**, 15–24.
14. Turgeon R. 2010 The role of phloem loading reconsidered. *Plant Physiol.* **152**, 1817–1823. (doi:10.1104/pp.110.153023)
15. Rennie EA, Turgeon R. 2009 A comprehensive picture of phloem loading strategies. *Proc. Natl Acad. Sci. USA* **106**, 14 162–14 167. (doi:10.1073/pnas.0902279106)
16. Liesche J, Martens HJ, Schulz A. 2011 Symplasmic transport and phloem loading in gymnosperm leaves. *Protoplasma* **248**, 181–190. (doi:10.1007/s00709-010-0239-0)
17. Sevanto S. 2014 Phloem transport and drought. *J. Exp. Bot.* **65**, 1751–1759. (doi:10.1093/jxb/ert467)
18. Choat B *et al*. 2012 Global convergence in the vulnerability of forests to drought. *Nature* **491**, 752–755.
19. West GB. 1999 The fourth dimension of life: fractal geometry and allometric scaling of organisms. *Science* **284**, 1677–1679. (doi:10.1126/science.284.5420.1677)
20. Savage VM, Bentley LP, Enquist BJ, Sperry JS, Smith DD, Reich PB, Framework T. 2010 Hydraulic trade-offs and space filling enable better predictions of vascular structure and function in plants. *Proc. Natl Acad. Sci. USA* **107**, 22 722–22 727. (doi:10.1073/pnas.1012194108)
21. Katifori E, Szöllősi GJ, Magnasco MO. 2010 Damage and fluctuations induce loops in optimal transport networks. *Phys. Rev. Lett.* **104**, 048704. (doi:10.1103/PhysRevLett.104.048704)
22. Corson F. 2010 Fluctuations and redundancy in optimal transport networks. *Phys. Rev. Lett.* **104**, 048703. (doi:10.1103/PhysRevLett.104.048703)
23. Zwieniecki MA, Stone HA, Leigh A, Boyce CK, Holbrook NM. 2006 Hydraulic design of pine needles: one-dimensional optimization for single-vein leaves. *Plant, Cell Environ.* **29**, 803–809. (doi:10.1111/j.1365-3040.2005.01448.x)
24. Noblin X, Mahadevan L, Coomaraswamy IA, Weitz DA, Holbrook NM, Zwieniecki MA. 2008 Optimal vein density in artificial and real leaves. *Proc. Natl Acad. Sci. USA* **105**, 9140–9144. (doi:10.1073/pnas.0709194105)
25. Colbert JT, Evert RF. 1982 Leaf vasculature in sugarcane (*Saccharum officinarum* L.). *Planta* **156**, 136–151. (doi:10.1007/BF00395428)
26. Russell S, Evert RF. 1985 Leaf vasculature in *Zea mays* L. *Planta* **164**, 448–458. (doi:10.1007/BF00395960)
27. Dannenhoffer JM, Ebert Jr W, Evert RF. 1990 Leaf vasculature in barley, *Hordeum vulgare* (Poaceae). *Am. J. Bot.* **77**, 636–652. (doi:10.2307/2444810)
28. Knoblauch M, Froelich DR, Pickard WF, Peters WS. 2014 SEORious business: structural proteins in sieve tubes and their involvement in sieve element occlusion. *J. Exp. Bot.* **65**, 79–93. (doi:10.1093/jxb/eru071)
29. Cath T, Childress A, Elimelech M. 2006 Forward osmosis: principles, applications, and recent

developments. *J. Membr. Sci.* **281**, 70–87. (doi:10.1016/j.memsci.2006.05.048)

30. Katifori E, Magnasco MO. 2012 Quantifying loopy network architectures. *PLoS ONE* **7**, e37994. (doi:10.1371/journal.pone.0037994)
31. Murray CD. 1926 The physiological principle of minimum work: I. The vascular system and the cost of blood volume. *Proc. Natl Acad. Sci. USA* **12**, 207–214. (doi:10.1073/pnas.12.3.207)
32. Murray CD. 1926 The physiological principle of minimum work: II. Oxygen exchange in capillaries. *Proc. Natl Acad. Sci. USA* **12**, 299–304. (doi:10.1073/pnas.12.5.299)
33. Jensen KH, Zwieniecki MA. 2013 Physical limits to leaf size in tall trees. *Phys. Rev. Lett.* **110**, 018104. (doi:10.1103/PhysRevLett.110.018104)
34. McCulloh KA, Sperry JS, Adler FR. 2003 Water transport in plants obeys Murray's law. *Nature* **421**, 939–942. (doi:10.1038/nature01444)
35. Rinaldo A, Rodriguez-Iturbe I, Rigon R, Bras RL, Ijjasz-Vasquez E, Marani A. 1992 Minimum energy and fractal structures of drainage networks. *Water Resour. Res.* **28**, 2183–2195. (doi:10.1029/92WR00801)
36. Bejan A, Lorente S. 2011 The constructal law and the evolution of design in nature. *Phys. Life Rev.* **8**, 209–240. (doi:10.1016/j.plrev.2011.05.010)
37. Bejan A, Lorente S, Lee J. 2008 Unifying constructal theory of tree roots, canopies and forests. *J. Theor. Biol.* **254**, 529–540. (doi:10.1016/j.jtbi.2008.06.026)
38. Bernot M, Caselles V, Morel JM. 2009 *Optimal transportation networks: models and theory*. Berlin, Germany: Springer.